

LETTER TO THE EDITOR

# Old massive clusters (and a nuclear star cluster?) in the tidal tails of NGC5238

M. Bellazzini<sup>1</sup>, F. Annibali<sup>1</sup>, M. Correnti<sup>2,6</sup>, M. Gatto<sup>3</sup>, M. Marinelli<sup>4</sup>, R. Pascale<sup>1</sup>, E. Sacchi<sup>5</sup>, M. Tosi<sup>1</sup>, M. Cignoni<sup>7,8</sup>, J.M. Cannon<sup>9</sup>, L. Schisgal<sup>9</sup>, G. Bortolini<sup>10</sup>, A. Aloisi<sup>11,4</sup>, G. Beccari<sup>12</sup>, and C. Nipoti<sup>13</sup>

<sup>1</sup> INAF - Osservatorio di Astrofisica e Scienza dello Spazio di Bologna, via Piero Gobetti 93/3, 40129 Bologna, Italy

<sup>2</sup> INAF - Osservatorio Astronomico di Roma, Via Frascati 33, 00078, Monteporzio Catone, Rome, Italy

<sup>3</sup> INAF - Osservatorio Astronomico di Capodimonte, Via Moiariello, 16, 80131 Napoli, Italy

<sup>4</sup> Space Telescope Science Institute 3700 San Martin Drive Baltimore, MD 21218, USA

<sup>5</sup> Leibniz-Institut für Astrophysik Potsdam (AIP), An der Sternwarte 16, 14482 Potsdam, Germany

<sup>6</sup> ASI-Space Science Data Center, Via del Politecnico, I-00133, Rome, Italy

<sup>7</sup> Department of Physics – University of Pisa, Largo B. Pontecorvo 3, 56127 Pisa, Italy

<sup>8</sup> INFN, Largo B. Pontecorvo 3, 56127, Pisa, Italy

<sup>9</sup> Macalester College, 1600 Grand Avenue, Saint Paul, MN 55105, USA

<sup>10</sup> Department of Astronomy, Stockholm University, AlbaNova University Center

<sup>11</sup> Astrophysics Division, Science Mission Directorate, NASA Headquarters, 300 E Street SW, Washington, DC 20546, USA

<sup>12</sup> European Southern Observatory, Karl-Schwarzschild-Strasse 2, 85748 Garching bei München, Germany

<sup>13</sup> Dipartimento di Fisica e Astronomia “Augusto Righi”, Università di Bologna, Via Gobetti 93/2, 40129 Bologna, Italy

Accepted for publication on September 15, 2024

## ABSTRACT

New, deep HST photometry allowed us to identify and study eight compact and bright ( $M_V \leq -5.8$ ) star clusters in the outskirts of the star-forming isolated dwarf galaxy NGC 5238 ( $M_* \approx 10^8 M_\odot$ ). Five of these clusters are new discoveries, and six appear projected onto, and/or aligned with the tidal tails recently discovered around this galaxy. The clusters are partially resolved into stars and their colour magnitude diagrams reveal a well developed red giant branch, implying ages older than 1-2 Gyr. Their integrated luminosity and structural parameters are typical of classical globular clusters and one of them has  $M_V = -10.56 \pm 0.07$ , as bright as  $\omega$  Cen, the brightest globular cluster of the Milky Way. Since the properties of this cluster are in the range spanned by those of nuclear star clusters we suggest that it may be the nuclear remnant of the disrupted satellite of NGC 5238 that produced the observed tidal tails.

**Key words.** Galaxies: dwarf – Galaxies: individual: NGC 5238 – Galaxies: interactions – Galaxies: star clusters: general

## 1. Introduction

The current  $\Lambda$  - Cold Dark Matter paradigm predicts that galaxies form by means of a hierarchical merging process (Primack 2024) irrespective of the mass scale of the galaxies over a very wide range (Diemand et al. 2005; Wang et al. 2020). Hence, the paradigm must be tested at any scale, including the smallest ones, that is in the realm of dwarf galaxies. Here the test is especially challenging, due to the intrinsic faint and low surface brightness nature of the dwarfs and of their possible satellites. However, systematic searches among local unresolved galaxies begin to provide interesting results (Paudel et al. 2018; Kado-Fong et al. 2020).

In this context, the Smallest Scale of the Hierarchy survey (SSH; Annibali et al. 2020) is aimed at searching for signs of recent interactions or merging with satellites in a sample of nearby ( $D \lesssim 10$  Mpc) isolated and (at least partially) resolved dwarf galaxies by tracing their stellar structure by star counts down to a very low surface brightness level ( $\mu_r \lesssim 31$  mag/arcsec<sup>2</sup>). While requiring that the galaxies can be resolved into stars strongly limits the accessible volume, it allows to discriminate between young stars, that trace the (typically) strongly asymmetric distribution of star forming regions, and old stars, specifically Red Giant Branch (RGB) stars (age  $\gtrsim 1 - 2$  Gyr), whose distribution

should reliably trace the galaxy gravitational potential and the possible disturbances induced by interactions with satellites.

Recently, Sacchi et al. (2024) reported on the discovery of prominent asymmetric extended features in the distribution of RGB stars in the outskirts of six SSH dwarfs, all interpreted as relics of the interaction with and ingestion of a former satellite (e.g., similarly to the case of DDO68, see Annibali et al. 2016, 2019). Among these, the star forming galaxy NGC 5238 ( $D \approx 4.5$  Mpc,  $M_* \approx 10^8 M_\odot$ ; Cannon et al. 2016, see Appendix A) was shown to display two wide asymmetric stellar features protruding from the northern and the southern edges of the regular ellipsoidal main body of the galaxy as traced by RGB stars (see Fig. 1, right panel). The northern feature ends with a kind of shell with a sharp edge in surface density, somehow bending to the south-west. To follow up this intriguing case of ingestion of a satellite by a dwarf we obtained deep Hubble Space Telescope (HST) observations covering the entire body of the galaxy as well as the tidal tails (program GO-17140<sup>1</sup>; P.I. F. Annibali). Inspecting the mosaic of Advanced Camera for Surveys - Wide Field Channel (ACS-WFC) images we noted, in the

<sup>1</sup> The images of NGC 5238 from this programme have been used for a beautiful ESA image of the week; <https://esahubble.org/images/potw2429a/>

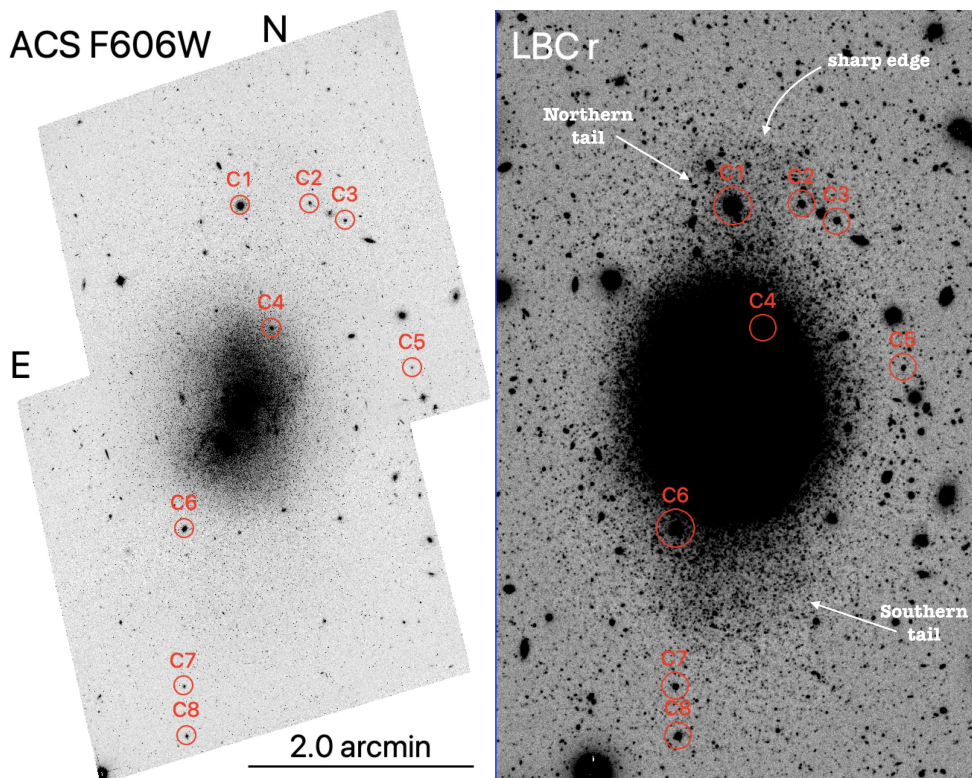


**Fig. 1.** Images of NGC 5238 from our HST (left image) and LBT (right image) data, with the star clusters considered in this letter circled and labelled. The different intensity cuts in the two images are intended to highlight the irregular structure of the inner star forming region (ACS image) and the regular ellipsoid of the main body as well as the shape of the tidal features protruding from its northern and southern edges (LBC image).

outskirts of the galaxy, eight obvious bright, compact and partially resolved star clusters, five of which were previously unknown. Their Colour Magnitude Diagram (CMD) suggests an old age for all of them. The newly discovered clusters, and the outermost one among those already known, lie far beyond the main body of the galaxy and appear to correlate with the tidal tails. One of them lies straight within the northern tail, at least in projection, and is as bright as the brightest globular cluster (GC) of the Milky Way (MW), showcasing properties typical of Nuclear Star Clusters (NSC; Neumayer et al. 2020, N20 hereafter). In this letter we report on these newly discovered clusters and their relation with the tidal tails of NGC 5238.

## 2. Analysis

The star cluster population in the main body of NGC 5238 has been systematically studied by the LEGUS HST Treasury Program (PI D. Calzetti) with an automatic pipeline (Adamo et al. 2017). Ages were estimated by fitting Spectral Energy Distribution (SED) models to the set of available HST magnitudes, that vary from cluster to cluster. The vast majority of the LEGUS candidate clusters unfortunately were classified as low-quality candidates, and only nine were confirmed by visual inspection as likely genuine clusters (Adamo et al. 2017; Cook et al. 2019, 2023). All of these nine have estimated ages  $\leq 2 \times 10^8$  yr, according to the LEGUS catalogue<sup>2</sup> and, above all, are deeply embedded into the main body of the galaxy. We will re-consider these inner clusters at the light of our new data in a future con-

tribution where we will study in detail the star formation and the morphology of the galaxy.

The final mosaics of drizzled ACS-WFC images of NGC 5238 we inspected summed a total exposure time of 13824 s in F606W and 22698.5 s in F814W. The F606W image is reproduced in the left panel of Fig. 1, flanked, on the right panel, by the SSH r band image from Sacchi et al. (2024) obtained with the Large Binocular Camera (LBC; Giallongo et al. 2008) mounted on the Large Binocular Telescope (LBT<sup>3</sup>), exactly on the same scale. The LBC image highlights the regular shape of the ellipsoidal main body of the galaxy and the two tails protruding from its northern and southern edges, while the intensity cuts of the ACS image have been set to reveal the complex morphology of the innermost star-forming regions. In both images we have encircled and labelled the bright and compact star clusters that we clearly identified on our ACS image as partially resolved into stars. Three of them, C4, C6 and C7, were already included in the LEGUS catalogue of candidate star clusters in NGC 5238<sup>4</sup>, while the other five are new discoveries, as they all lie beyond the footprint of the LEGUS images of this galaxy. Stamp images zoomed on the clusters can be found in Appendix C.

We used the Aperture Photometry Tool (APT; Laher et al. 2012a,b) to estimate the cluster centres and to get surface aperture photometry on circular apertures for all the eight clusters. Throughout the paper we always report F606W and F814W magnitudes in the VEGAMAG system (Sirianni et al. 2005; Bedin et al. 2005). The integrated magnitude in F606W and F814W

<sup>2</sup> We used the reference LEGUS catalogue, that is the one that uses Milky Way extinction, averaged aperture correction method, and Padova stellar evolutionary tracks (see [https://archive.stsci.edu/prepds/legus/cluster\\_catalogs/ngc5238.html](https://archive.stsci.edu/prepds/legus/cluster_catalogs/ngc5238.html)).

<sup>3</sup> <https://www.lbto.org>

<sup>4</sup> C6 = LEGUS 591 is among the nine confirmed LEGUS candidates, while the other two clusters in common with our sample did not pass the cut for further visual inspection in the LEGUS pipeline.



**Table 1.** Compact clusters in the outskirts of NGC5238.

| SSH<br>id | ra<br>[deg] | dec<br>[deg] | F606W<br>[mag] | F814W<br>[mag] | $M_V$<br>[mag] |
|-----------|-------------|--------------|----------------|----------------|----------------|
| C1        | 203.67842   | 51.64420     | 17.34±0.02     | 16.60±0.02     | -10.56±0.05    |
| C2        | 203.66194   | 51.64461     | 20.98±0.09     | 20.17±0.09     | -6.89±0.12     |
| C3        | 203.65347   | 51.64202     | 20.04±0.06     | 19.34±0.06     | -7.87±0.08     |
| C4 (11)   | 203.67096   | 51.62609     | 19.39±0.04     | 18.65±0.05     | -8.52±0.07     |
| C5        | 203.63766   | 51.62032     | 22.05±0.15     | 21.25±0.15     | -5.83±0.18     |
| C6 (591)  | 203.69168   | 51.59655     | 18.35±0.03     | 17.61±0.03     | -9.55±0.06     |
| C7 (617)  | 203.69176   | 51.57332     | 21.26±0.10     | 20.50±0.11     | -6.63±0.13     |
| C8        | 203.69113   | 51.56597     | 19.74±0.05     | 19.02±0.06     | -8.17±0.06     |

**Notes.** Numbers in parentheses in the first column are LEGUS id numbers, when available. Coordinates are J2000 as embedded in the drizzled F606W image. Magnitudes have been computed over circular apertures of radius  $r = 6.5''$  for C1,  $r = 2.0''$  for C4 and C5, and  $r = 3.0''$  for all the remaining clusters.

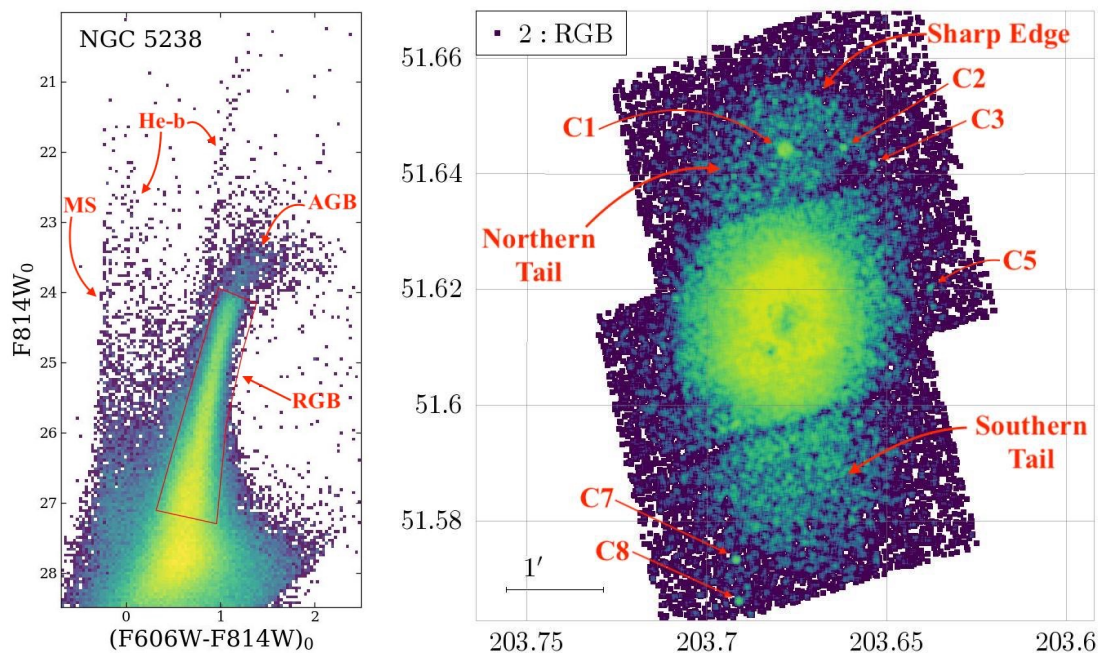


**Fig. 2.** Left panel: CMD of NGC 5238 from our HST ACS-WFC photometry (entire sample). The main evolutionary phases are labelled and the RGB selection box is plotted in red. Right panel: map of the RGB stars in our field (RA and Dec in degrees). Each star is colour coded according to the local density. The main tidal features are labelled as well as all the star clusters possibly associated with them, that appear as local overdensities in the map. Please note how prominent is the overdensity associated to C1. The two diagonal under-dense stripes correspond to the gaps between the ACS-WFC CCDs in the two WFC images used to build our mosaic image. In these stripes the effective exposure time is lower than elsewhere.

was obtained using apertures large enough to include also the contribution of the resolved stars in the cluster outskirts (see Tab. 1). The background flux to be subtracted was estimated in large concentric annuli to include the contribution of resolved stars in the field of NGC 5238 as well as of background sources (the field is rich of distant galaxies). The coordinates of the clusters and their integrated magnitudes obtained in this way are reported in Table 1. The magnitudes of C4 and C6 are in good agreement with those measured by the LEGUS pipeline (based on SExtractor; Bertin & Arnouts 1996, see App. D), while for C7 they provide values fainter than ours by about two magnitudes, in both passbands, clearly not compatible with the observed cluster. When reducing our ACS images with SExtractor we noted that this relatively sparse and resolved cluster was split by the code into (at least) two fainter sources. This behaviour is likely

at the origin of the underestimate of the integrated flux of C7 by LEGUS.

The clusters' surface brightness (SB) profiles were obtained by aperture photometry on circular annuli with APT. We determined the structural parameters of the clusters in two ways, on the F606W profiles. First, we fitted the observed surface brightness (SB) profiles with King (1966, K66 hereafter) single-mass models convoluted with a simple model of the ACS Point Spread Function (PSF), as done in Federici et al. (2007); Barmby et al. (2007). The central SB was fixed at the value of the innermost point of the observed profile and then we searched for the values of the core radius ( $r_c$ ) and of the concentration parameter ( $C = \log(r_t/r_c)$ , where  $r_t$  is the tidal radius, see K66) that minimises  $\chi^2$ . Second, we fitted straight Elson et al. (1987, EFF87) models to the observed profiles with the curve fit Python library, as done in Gatto et al. (2021). The observed profiles of the clus-

ters, their best fitting curves and the resulting structural parameters are presented and briefly discussed in App. D. The two sets of models perform very similarly in the innermost regions of the clusters, while EFF87 appears much better in reproducing the extended outer regions of the clusters. In particular, the external parts of the profiles of C1, C3 and C8 do not seem compatible with tidal truncation, as typical of clusters in dwarf galaxies (EFF87, Gatto et al. 2021, and references therein). It is reassuring to note that integrating the EFF87 profiles we get integrated magnitudes in excellent agreement with those reported in Tab. 1. On the other hand, core and half-light radii from the fit of K66 model must be considered as our best estimates of the true cluster size since in this case the effect of the PSF is taken into account.

Stellar PSF photometry was obtained using the latest version of DOLPHOT (Dolphin 2000, 2016), following the approach described in Annibali et al. (2019) and the set-up by Williams et al. (2014). Additional details and the adopted selections are described in App. B. In the left panel of Fig. 2 we show the CMD of the entire ACS sample, that is dominated by a prominent RGB, tipping around  $F814W_0 \approx 24.1$  and  $(F606W-F814W)_0 \approx 1.0$ . A significant population of Asymptotic Giant Branch (AGB) stars, tracing intermediate-age populations, is clearly visible above the RGB tip. At colours bluer than the RGB, the sequences of red and blue young core He-burning (He-b) stars can be easily identified, as well as the young Main Sequence (MS), clearly marking the blue edge of the CMD for  $F814W_0 \lesssim 27.0$ . Thanks to the quality of our data, it is easy to select RGB stars on this CMD to obtain a map of the oldest populations that can be identified in our data, displayed in the right panel of Fig. 2. Both the southern and the northern tidal tails are clearly evident in the map, as well as the SW-bending sharp edge of the latter (please, compare with Fig. 1, right panel). It is extremely interesting and somehow striking, given the distance of the galaxy, that six of the eight clusters listed in Tab. 1 are readily visible in the map as small scale overdensities of RGB stars: the five newly discovered clusters (C1, C2, C3, C5, and C8) and the outermost cluster already found by LEGUS, C7. The CMD of small circular fields around these clusters are shown in Fig. C.2 and compared with the CMD of control fields. The comparisons fully support the idea that the clusters are likely old and metal-poor (albeit in some of them the presence of intermediate-age AGB stars cannot be excluded, see App. C). It is intriguing to note that C1, C2 and C3 are projected onto the northern tail, somehow following the bending of its sharp edge. The position of C5 is not incompatible with the possible southward prolongation of the Northern tail<sup>5</sup>. C7 and C8 lie just beyond the south-east edge of the Southern tail. In the following we will focus our attention on these six clusters as they are those most likely associated with the tidal tails<sup>6</sup>. In the following we will adopt  $D = 4.17 \pm 0.10$  Mpc and  $E(B-V)=0.01$  (see App. E).

It is worth noting that the entire field of view spanned by our ACS images, with a maximum projected distance from the galaxy centre of  $\approx 6.3$  kpc, is dominated by stars of NGC 5238.

<sup>5</sup> Some of the LEGUS candidate clusters look intriguingly aligned in a north-south narrow sheet southward of C5 and close to C7 and C8, but all of them were classified as low-quality candidates. Indeed, a close inspection of our images confirmed that they actually are background/foreground objects.

<sup>6</sup> Although they do not emerge as obvious overdensities over the strong background of stars in the main body of the galaxy in Fig. 2, also the CMDs of C4 and C6 are dominated by RGB stars and their properties are also typical of classical GCs. The optical spectrum of C6 provided by the Sloan Digital Sky Survey DR17 (Ahumada et al. 2020) suggests that the cluster should have an age in the range 1-4 Gyr.

This means that the tidal tails are immersed into a vaster, low SB halo of which we do not detect the end, where additional star clusters may lie.

### 3. Discussion and conclusion

To derive absolute integrated magnitudes in the V band, we transformed the ACS magnitudes into V using Eq. 1 of Galleti et al. (2006). The clusters in Tab.1 have  $-5.8 \leq M_V \leq -10.5$  and half-light radii  $3.4 \text{ pc} \leq R_h \leq 14.5 \text{ pc}$ , within the range spanned by classical GCs (see Fig. 3). Adopting the mean mass-to-light ratio of Galactic GCs ( $M/L_V = 1.8$ , Baumgardt et al. 2020), the estimated masses lie in the range  $4.5 \leq \log(M/M_\odot) \leq 6.4$ . We verified that they follow all the GC scaling relations that we were able to check (e.g. C vs.  $r_c$ , C vs.  $M_V$ , etc.; Djorgovski et al. 2003). Their mean colours as well as their CMD are typical of old and mildly metal-poor globular clusters. The fact that six of these bright GCs lie in the extreme outskirts of the galaxy and are correlated (in projection) with the prominent tidal tails discovered by Sacchi et al. (2024) may suggest that they were associated with the destroyed satellite that produced the tails. We have clear examples of GCs lying within tidal tails, and therefore being accreted into a larger galaxy along tidal tails, around the MW (e.g., Bellazzini et al. 2020, and references therein) and M31 (Mackey et al. 2019) but, to the best of our knowledge, this is the first case in which this is observed to occur in a dwarf galaxy (while accretion of clusters in a dwarf have been suggested by Hwang et al. 2014, for NGC 6822).

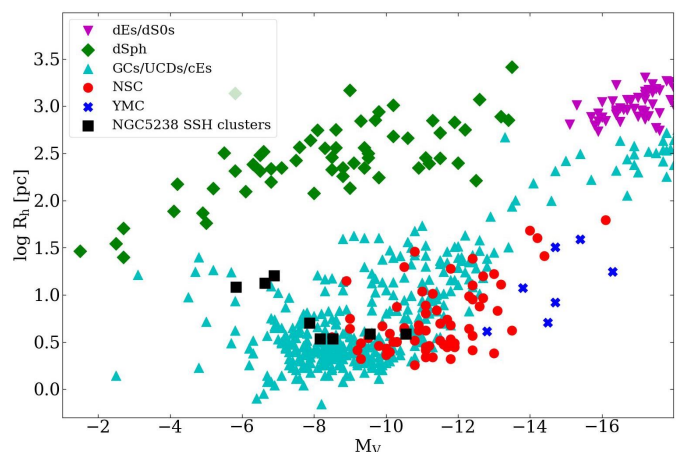


**Fig. 3.** NGC 5238 clusters listed in Tab. 1 are compared to the sample of pressure-supported stellar systems from Norris et al. (2014) in the plane opposing the logarithm of  $R_h$  to the absolute integrated V magnitude. The Norris et al. (2014) catalogue does not discriminate between GCs, UCDs and compact ellipticals (cEs) but the distribution of the GC/UCD/cE class is dominated by UCDs and cEs for  $M_V \leq -10.0$  and by GCs for  $M_V > -10.0$ .

The case of C1 is especially intriguing in this sense. C1, located straight in the middle of the Northern tail, has an absolute integrated V magnitude  $M_V = -10.56 \pm 0.07$  that is very similar to that of  $\omega$  Cen ( $M_V = -10.51 \pm 0.05$  Baumgardt et al. 2020; Baumgardt & Vasiliev 2021)<sup>7</sup>, the brightest GC of the Milky Way, a galaxy with a GC system of more than 150 members and whose stellar mass is  $\approx 500$  times larger than that of

<sup>7</sup> <https://people.smp.uq.edu.au/HolgerBaumgardt/globular/>

NGC 5238 (Bland-Hawthorn & Gerhard 2016).  $\omega$  Cen is generally believed to be the nuclear remnant of a former, and now disrupted, satellite of the MW (Ibata et al. 2019), in analogy with the case of another very bright GC, M 54 ( $M_V = -9.99 \pm 0.07$ ), that is part of the stellar nucleus of the disrupting Sgr dSph galaxy (Bellazzini et al. 2008; Carretta et al. 2010; Alfaro-Cuello et al. 2019, 2020). Indeed, Fig. 3 shows that C1 lies in the region of the  $M_V - \log(R_h)$  plane that is dominated by faint NSCs and Ultra Compact Dwarf galaxies (UCD; at least some of which may be the compact central remnant of tidally stripped galaxies; Misgeld & Hilker 2011; Mieske et al. 2013, N20). In particular, its luminosity and size are typical of stellar nuclei in dwarf galaxies ( $M_\star < 10^9 M_\odot$ ; see Tab 2 of N20). Also the low ellipticity,  $\epsilon = 0.07 \pm 0.01^8$ , is typical of low mass NSCs. It is tantalising to hypothesise that C1 was in fact the nuclear remnant of the dwarf satellite that was disrupted in the interaction with NGC 5238, producing the tidal tails. Indeed this appears as the most likely explanation for the presence of such a massive star cluster so far away from the centre of a dwarf galaxy ( $\approx 2.5$  kpc, in projection, more than five times the galaxy  $R_h^9$ ). In this context it is also worth recalling another case of a possible nuclear remnant found into the outskirts of a dwarf galaxy, CL77 in NGC 4449, reported by Annibali et al. (2012), as well as the examples of UCDs caught in the process of formation by tidal shredding around spiral galaxies reported by Jennings et al. (2015) and Paudel et al. (2023). The case of NGC3628-UCD1 is particularly interesting, as the system is embedded in a tidal tail and it is remarkably similar to C1 in size and luminosity. NGC 5238 hosts another star cluster of comparable brightness as C1 close to its optical centre, LEGUS 242 with  $M_V = -10.7 \pm 0.3$  (from LEGUS photometry). However, this cluster has a much bluer colour than C1,  $(F606W - F814W)_0 = 0.43 \pm 0.12$  vs.  $(F606W - F814W)_0 = 0.73 \pm 0.03$  and appear to be associated with very strong nebular emission (Cannon et al. 2016). LEGUS reports a very young age for this cluster ( $10^6 - 10^7$  yr, depending on the version of the catalogue) and, consequently a relatively low mass  $M \lesssim 5 \times 10^4 M_\odot$ .

At this stage, only speculations based on uncertain assumptions can be made on the nature of the hypothesised progenitor of C1. According to the relation between the stellar masses of NSCs and the host galaxies (Eq. 1 of N20), if C1 is a stripped NSC the most likely mass of its parent galaxy is  $M_\star \approx 10^{8.7} M_\odot$  but, given the large scatter of the relation, progenitor masses down to  $M_\star \approx 10^{7.0} - 10^{8.0} M_\odot$  are also possible (see also Lambert et al. 2024), that would imply a (stellar) mass ratio in the range  $\sim 0.1 - 1$  for the merging event, assuming, for simplicity, that the two interacting galaxies have the same M/L ratio. Assuming that the six clusters in the tidal tails belonged to the disrupted satellite, its GC specific frequency ( $S_N$ , see Brodie & Strader 2006), will fall within the range observed in nucleated dwarf with  $M_V \gtrsim -14.5$  for stellar mass ratios  $\gtrsim 0.2$  (Miller & Lotz 2007). A lower mass ratio for the merging is possible, e.g., if C1 is itself a low-mass UCD (Saifollahi et al. 2021), in which case it would be difficult to explain the presence of the other clusters in the tails.

The tentative model of NGC5238 and its tails by Pascale et al. (2024) was only constrained by the apparent surface density distribution and by the H $\alpha$  kinematics. The discovery of these bright clusters in the tidal tails opens the path for obtaining

new and more powerful constraints, e.g., by using the clusters to probe the stellar velocity field in the tails, thus opening a powerful window on the rare and fascinating case of nearby merging between dwarf galaxies.

*Acknowledgements.* We are grateful to Angela Adamo and David Cook for their help and assistance in the use of LEGUS catalogues. MB and FA acknowledge financial support to this project by INAF, through the PRIN-2023 grant Ob. Fu 1.05.23.05.09 "Dwarf galaxies as probes of the Lambda Cold Dark Matter hierarchical paradigm at the smallest scales" (P.I.: F. Annibali). M. Correnti acknowledge financial support from the ASI-INAF agreement n.2022-14-HH-0. M. Cignoni acknowledges the support of INFN "iniziativa specifica TAsP". MG acknowledges the INAF AstroFit grant Fu Ob. 1.05.11. RP acknowledge the financial support to this research by the Italian Research Center on High Performance Computing Big Data and Quantum Computing (ICSC), project funded by European Union - NextGenerationEU - and National Recovery and Resilience Plan (NRRP) - Mission 4 Component 2 within the activities of Spoke 3 (Astrophysics and Cosmos Observations). These data are associated with the HST GO program 17140 (PI: F. Annibali). Support for program number 17140 was provided by NASA through a grant from the Space Telescope Science Institute, which is operated by the Association of Universities for Research in Astronomy under NASA contract This work is based on LBT data. The LBT is an international collaboration among institutions in the United States, Italy, and Germany. LBT Corporation partners are the University of Arizona on behalf of the Arizona Board of Regents; Istituto Nazionale di Astrofisica, Italy; LBT Beteiligungsgesellschaft, Germany, representing the Max Planck Society, the Leibniz Institute for Astrophysics Potsdam, and Heidelberg University; the Ohio State University, and the Research Corporation, on behalf of the University of Notre Dame, University of Minnesota, and University of Virginia. We acknowledge the support from the LBT-Italian Coordination Facility for the execution of observations, data distribution, and reduction. This research has made use of the SIMBAD database, operated at CDS, Strasbourg, France. This research has made use of the NASA/IPAC Extragalactic Database (NED), which is operated by the Jet Propulsion Laboratory, California Institute of Technology, under contract with the National Aeronautics and Space Administration. In this analysis we made use of TOPCAT (<http://www.starlink.ac.uk/topcat/>, Taylor 2005), APT (<https://www.aperturephotometry.org> Laher et al. 2012a,b), DOLPHOT (<http://americano.dolphinim.com/dolphot/>, Dolphin 2000, 2016).

## References

- Adamo, A., Ryon, J. E., Messa, M., et al. 2017, *ApJ*, 841, 131  
 Ahumada, R., Allende Prieto, C., Almeida, A., et al. 2020, *ApJ*, 249, 3  
 Aihara, H., Allende Prieto, C., An, D., et al. 2011, *ApJS*, 193, 29  
 Alfaro-Cuello, M., Kacharov, N., Neumayer, N., et al. 2020, *ApJ*, 892, 20  
 Alfaro-Cuello, M., Kacharov, N., Neumayer, N., et al. 2019, *ApJ*, 886, 57  
 Annibali, F., Beccari, G., Bellazzini, M., et al. 2020, *MNRAS*, 491, 5101  
 Annibali, F., Bellazzini, M., Correnti, M., et al. 2019, *ApJ*, 883, 19  
 Annibali, F., Nipoti, C., Ciotti, L., et al. 2016, *ApJ*, 826, L27  
 Annibali, F., Tosi, M., Aloisi, A., van der Marel, R. P., & Martinez-Delgado, D. 2012, *ApJ*, 745, L1  
 Barmby, P., McLaughlin, D. E., Harris, W. E., Harris, G. L. H., & Forbes, D. A. 2007, *AJ*, 133, 2764  
 Baumgardt, H., Sollima, A., & Hilker, M. 2020, *PASA*, 37, e046  
 Baumgardt, H. & Vasiliev, E. 2021, *MNRAS*, 505, 5957  
 Bedin, L. R., Cassisi, S., Castelli, F., et al. 2005, *MNRAS*, 357, 1038  
 Bellazzini, M., Ibata, R., Malhan, K., et al. 2020, *A&A*, 636, A107  
 Bellazzini, M., Ibata, R. A., Chapman, S. C., et al. 2008, *AJ*, 136, 1147  
 Bellazzini, M. & Pascale, R. 2024, *A&A*, in press, arXiv:2406.04781  
 Bellazzini, M., Perina, S., Galletti, S., & Oosterloo, T. 2011, *A&A*, 533, A37  
 Bertin, E. & Arnouts, S. 1996, *A&AS*, 117, 393  
 Bland-Hawthorn, J. & Gerhard, O. 2016, *ARA&A*, 54, 529  
 Bressan, A., Marigo, P., Girardi, L., et al. 2012, *MNRAS*, 427, 127  
 Brodie, J. P. & Strader, J. 2006, *ARA&A*, 44, 193  
 Cannon, J. M., McNichols, A. T., Teich, Y. G., et al. 2016, *AJ*, 152, 202  
 Carretta, E., Bragaglia, A., Gratton, R. G., et al. 2010, *ApJ*, 714, L7  
 Cook, D. O., Lee, J. C., Adamo, A., et al. 2023, *MNRAS*, 519, 3749  
 Cook, D. O., Lee, J. C., Adamo, A., et al. 2019, *MNRAS*, 484, 4897  
 Diemand, J., Moore, B., & Stadel, J. 2005, *Nature*, 433, 389  
 Djorgovski, S. G., Côté, P., Meylan, G., et al. 2003, in *Astronomical Society of the Pacific Conference Series*, Vol. 296, *New Horizons in Globular Cluster Astronomy*, ed. G. Piotto, G. Meylan, S. G. Djorgovski, & M. Riello, 479  
 Dolphin, A. 2016, *DOLPHOT: Stellar photometry*, *Astrophysics Source Code Library*, record ascl:1608.013  
 Dolphin, A. E. 2000, *PASP*, 112, 1383  
 Elson, R. A. W., Fall, S. M., & Freeman, K. C. 1987, *ApJ*, 323, 54  
 Federici, L., Bellazzini, M., Galletti, S., et al. 2007, *A&A*, 473, 429

<sup>8</sup> Average and standard deviation of the measures obtained from the F606W and F814W images with SExtractor.

<sup>9</sup> According to the  $R_h$  values reported in the NASA/IPAC Extragalactic Database <http://ned.ipac.caltech.edu>

- Fukugita, M., Ichikawa, T., Gunn, J. E., et al. 1996, *AJ*, 111, 1748
- Galletti, S., Federici, L., Bellazzini, M., Buzzoni, A., & Pecci, F. F. 2006, *ApJ*, 650, L107
- Gatto, M., Ripepi, V., Bellazzini, M., et al. 2021, *MNRAS*, 507, 3312
- Giallongo, E., Ragazzoni, R., Grazian, A., et al. 2008, *A&A*, 482, 349
- Hwang, N., Park, H. S., Lee, M. G., et al. 2014, *ApJ*, 783, 49
- Ibata, R. A., Bellazzini, M., Malhan, K., Martin, N., & Bianchini, P. 2019, *Nature Astronomy*, 3, 667
- Jennings, Z. G., Romanowsky, A. J., Brodie, J. P., et al. 2015, *ApJ*, 812, L10
- Kado-Fong, E., Greene, J. E., Greco, J. P., et al. 2020, *AJ*, 159, 103
- Karachentsev, I. D., Makarov, D. I., & Kaisina, E. I. 2013, *AJ*, 145, 101
- King, I. R. 1966, *AJ*, 71, 64
- Laher, R. R., Gorjian, V., Rebull, L. M., et al. 2012a, *PASP*, 124, 737
- Laher, R. R., Rebull, L. M., Gorjian, V., et al. 2012b, *PASP*, 124, 764
- Lambert, M., Khim, D. J., Zaritsky, D., & Donnerstein, R. 2024, *AJ*, 167, 61
- Mackey, A. D., Ferguson, A. M. N., Huxor, A. P., et al. 2019, *MNRAS*, 484, 1756
- Makarov, D. I., Makarova, L. N., & Uklein, R. I. 2013, *Astrophysical Bulletin*, 68, 125
- Marble, A. R., Engelbracht, C. W., van Zee, L., et al. 2010, *ApJ*, 715, 506
- Mieske, S., Frank, M. J., Baumgardt, H., et al. 2013, *A&A*, 558, A14
- Miller, B. W. & Lotz, J. M. 2007, *ApJ*, 670, 1074
- Misgeld, I. & Hilker, M. 2011, *MNRAS*, 414, 3699
- Moustakas, J. & Kennicutt, Robert C., J. 2006, *ApJS*, 164, 81
- Neumayer, N., Seth, A., & Böker, T. 2020, *A&A Rev.*, 28, 4
- Norris, M. A., Kannappan, S. J., Forbes, D. A., et al. 2014, *MNRAS*, 443, 1151
- Pascale, R., Annibali, F., Tosi, M., et al. 2024, *A&A*, 688, A144
- Paudel, S., Duc, P.-A., Lim, S., et al. 2023, *MNRAS*, 526, L136
- Paudel, S., Smith, R., Yoon, S. J., Calderón-Castillo, P., & Duc, P.-A. 2018, *ApJS*, 237, 36
- Peacock, M. B., Maccarone, T. J., Knigge, C., et al. 2010, *MNRAS*, 402, 803
- Primack, J. 2024, *ARA&A*, 74, 173
- Sabbi, E., Calzetti, D., Ubeda, L., et al. 2018, *ApJS*, 235, 23
- Sacchi, E., Bellazzini, M., Annibali, F., et al. 2024, *A&A*, in press, arXiv:2406.01683
- Saifollahi, T., Janz, J., Peletier, R. F., et al. 2021, *MNRAS*, 504, 3580
- Schlafly, E. F. & Finkbeiner, D. P. 2011, *ApJ*, 737, 103
- Schlegel, D. J., Finkbeiner, D. P., & Davis, M. 1998, *ApJ*, 500, 525
- Sirianni, M., Jee, M. J., Benítez, N., et al. 2005, *PASP*, 117, 1049
- Taylor, M. B. 2005, in *Astronomical Society of the Pacific Conference Series*, Vol. 347, *Astronomical Data Analysis Software and Systems XIV*, ed. P. Shopbell, M. Britton, & R. Ebert, 29
- Tully, R. B., Rizzi, L., Shaya, E. J., et al. 2009, *AJ*, 138, 323
- Vergely, J. L., Lallement, R., & Cox, N. L. J. 2022, *A&A*, 664, A174
- Wang, J., Bose, S., Frenk, C. S., et al. 2020, *Nature*, 585, 39
- Williams, B. F., Lang, D., Dalcanton, J. J., et al. 2014, *ApJS*, 215, 9

## Appendix A: Properties and isolation of NGC 5238

In table A.1 we summarise the main properties of NGC 5238, including the tidal indices defined by Karachentsev et al. (2013) to quantify the possible impact of tides from nearby galaxies (see Annibali et al. 2016, for a discussion related to the selection of SSH targets). Negative values of these indices imply that the effect of tidal forces from known surrounding galaxies is negligible.  $\theta_1$  is intended to measure the tidal force exerted on the galaxy by the main disturber while  $\theta_5$  combines the effects of the five strongest disturbers. It is interesting to note that both parameters are negative, in the case of NGC 5238.

NGC 5238 is a member of the Canes Venatici I Cloud (CVn I Cloud; Makarov et al. 2013) that includes several galaxies with distance and line of sight velocity very similar to it. However, according to Karachentsev et al. (2013) the main disturber of NGC 5238 is the Seyfert galaxy NGC 4736 (M 94) that lies  $\approx 13.0^\circ$  apart in projection, corresponding to  $\approx 960$  kpc. The closest dwarf galaxy is UGC 8331,  $\approx 5.1^\circ$  apart in projection, corresponding to  $\approx 370$  kpc. Assuming that this galaxy is exactly at the same line of sight distance as NGC 5238 and a transverse velocity two times the velocity dispersion of the CVn I Cloud ( $\sigma = 51$  km/s; Makarov et al. 2013), it would require  $\approx 3.5$  Gyr to bring the two galaxies at the same position. In summary, it seems highly unlikely that the existing galaxies around NGC 5238 can be responsible for its disturbed morphology; the galaxy appears to be remarkably isolated.

**Table A.1.** Main properties of NGC5238.

| Parameter                      | Value                             | Notes                                     |
|--------------------------------|-----------------------------------|---|
| $D$                            | $4.2 \pm 0.1$ Mpc                 | this work                                 |
| $M_V$                          | $-14.3 \pm 0.1$                   | HyperLeda <sup>a</sup>                    |
| $R_h$                          | $236 \pm 8$ pc                    | (major axis) NED <sup>b</sup>             |
| $M_\star$                      | $8.9 \times 10^7 M_\odot$         | Cannon et al. (2016)                      |
| $M_{H\text{I}}$                | $2.2 \pm 0.3 \times 10^7 M_\odot$ | Cannon et al. (2016)                      |
| $M_{\text{dyn}}$               | $3 \times 10^8 M_\odot$           | Cannon et al. (2016)                      |
| $12 + \log(\text{O}/\text{H})$ | $7.96 \pm 0.20$                   | Moustakas & Kennicutt (2006) <sup>c</sup> |
| $V_h$                          | $232 \pm 1$ km s <sup>-1</sup>    | Cannon et al. (2016)                      |
| $\theta_1$                     | -0.4                              | Karachentsev et al. (2013)                |
| $\theta_5$                     | -0.2                              | Karachentsev et al. (2013)                |

**Notes.** <sup>a</sup> <http://atlas.obs-hp.fr/hyperleda/>, from SDSS g and r magnitudes by Aihara et al. (2011) transformed as in App. D. <sup>b</sup> Nasa Extragalactic Database <http://ned.ipac.caltech.edu>, from SDSS DR5 measures. <sup>c</sup> See also Marble et al. (2010) and Cannon et al. (2016).  $V_h$  is the heliocentric line of sight velocity, measured with H I observations.

## Appendix B: Data reduction

We downloaded from the HST archive<sup>10</sup> the *flc* science images, which correspond to the bias-corrected, dark-subtracted, flat-fielded, CTE corrected, GAIA-aligned images. We combined them in a single-stacked, distortion-corrected image (to be used as a reference frame in the photometric data reduction). Then, we used the latest version of DOLPHOT (Dolphin 2000, 2016) to obtain simultaneous multi-filter PSF photometry. We set DOLPHOT parameters using a combination between the default values and those derived by (Williams et al. 2014).

<sup>10</sup> <https://mast.stsci.edu/portal/Mashup/Clients/Mast/Portal.html>

To exclude artifacts and spurious detections from the DOLPHOT output, we adopted a series of selection cuts using diagnostic parameters included in the photometric catalog (following, e.g., Annibali et al. 2019). In particular, after a first selection where we retained only the sources with `Object type`  $\leq 1$ , photometry quality `flag`  $\leq 2$ , and  $S/N > 3$ , we adopted cuts in the `sharp` parameter, tracing the difference in extension of the image of a source with respect to a point source, and in the `crowd` parameter, indicative of the degree of contamination by nearby stars, that allows to remove a large fraction of contaminants (see, e.g. Bellazzini et al. 2011, and references therein). The `sharp` cuts have been derived from the `sharp` vs magnitude distribution, selecting sources with  $|\text{sharp}| < 0.075$  or, after calculating the mean and sigma of the `sharp` distribution in 0.5 magnitudes bins, within  $\pm 2.0\sigma$  from the local mean. For the `crowd` parameter, we selected sources with `crowd`  $< 0.1$  or within  $2.0\sigma$  from the local mean, calculated from the mean and sigma of the `crowd` distribution in 0.5 magnitudes bins.

Additional details on the data reduction will be provided in a forthcoming paper where we will discuss in detail the structure and star formation history of the galaxy.



## Appendix C: Cluster images and CMDs

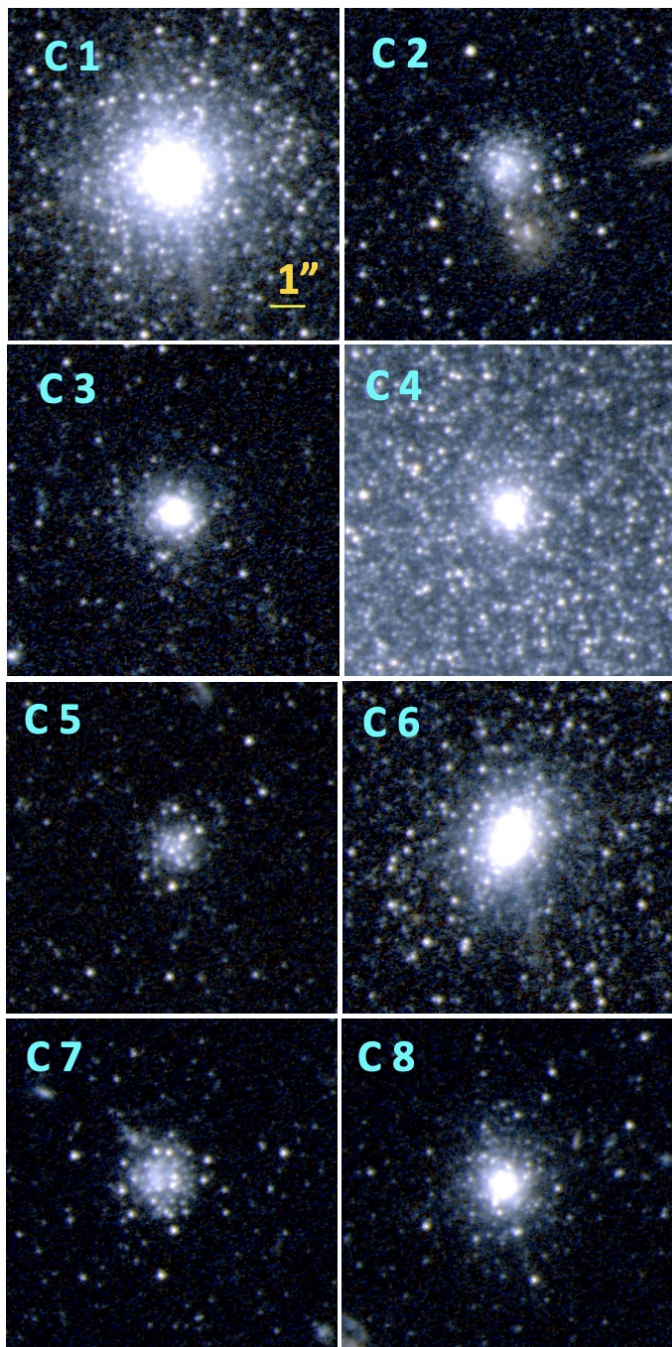


**Fig. C.1.** Stamp images zoomed on a  $10'' \times 10''$  box centred on the cluster for all the eight clusters listed in Tab. 1. North is up and East to the left. The RGB images have been obtained using the F814W image for the Red channel, the F606W image for the Blue channel, and the sum of the F814W and F606w images for the Green channel.

The RGB colour stamp images zoomed on the eight clusters listed in Tab. 1 are presented in Fig. C.1. There are several features that may be worth noting here: (a) the great extension of C1, with many well resolved stars in the outer regions, (b) the fact that all the clusters appear as partially resolved, (c) the background galaxy very close to C2, to the south-south-west of its centre, (d) the fact that C2, C5 and C7 are significantly less compact than the other five clusters, with bright stars resolved

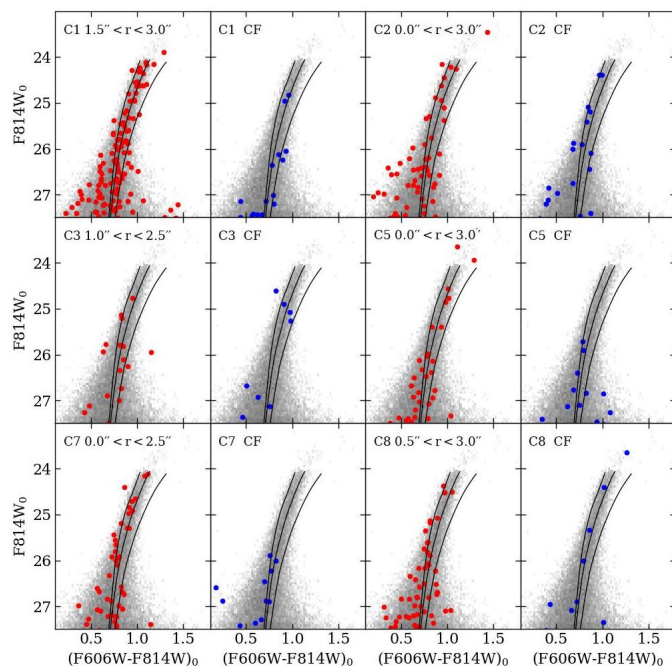


**Fig. C.2.** Colour magnitude diagrams for the six star clusters possibly associated with the tidal tails. In each panel the CMD of the field population in the outskirts of NGC 5238 ( $r > 70.0''$ ) is plotted in grey and the RGB of three Padova isochrones (Bressan et al. 2012) of age 12.0 Gyr and  $[M/H] = -2.2, -1.5, -1.0$  (from left to right) are plotted as black continuous curves, for reference. For each cluster, stars within a small radial annulus around the cluster centre are plotted as red circles in the "on cluster" CMD, while those of a nearby Control Field (CF) of the same area are plotted as blue circles in the flanking CMD. The limits of the radial annuli are reported in the "on cluster" panels.

also very close to the centre, (e) the remarkable elongation of C6 (see App. D). All these clusters appear as genuine GCs.

In Fig. C.2, for each of the six clusters possibly associated with the tidal tails, we show the CMD of the stars enclosed within the reported radial annulus centred on the cluster centre (left panels, red filled circles), flanked by the CMD of the stars located within an annulus of the same area but centred  $\approx 20''$  apart from the cluster (Control Field; CF), carefully avoiding possibly problematic regions (e.g. including bright foreground stars and/or bright or extended background galaxies). Both the stars in the cluster and in the CF region are superimposed to the CMD of the stars in the outskirts of the galaxy ( $r > 70.0''$ , grey dots), for reference. It may be worth noting that these regions of the galaxy are populated only by old (RGB) and intermediate-age (bright AGB) stars. We have also superimposed to each CMD the RGB of three theoretical isochrones from the Padova set Bressan et al. (2012)<sup>11</sup> of age 12.0 Gyr and  $[M/H] = -2.2, -1.5, -1.0$ , properly shifted to the distance of NGC 5238. From all the comparisons it emerges that the considered clusters are indeed over-densities of RGB stars with respect to the surrounding field, as shown already in Fig. 2, albeit in the case of the most compact cluster (C3) the statistical significance may be low due to the low number of individual stars that can be resolved in the cluster outskirts. In all cases the cluster stars are roughly enclosed between the  $[M/H] = -1.5$  and the  $[M/H] = -2.2$  isochrones, suggesting that the clusters, if old, are quite metal-poor. In the cluster regions of C1, C2 and C3 there are also one, one and two AGB stars

<sup>11</sup> <http://stev.oapd.inaf.it/cgi-bin/cmd>



brighter than the RGB tip, respectively, that have no counterpart in the CFs. This may suggest that these clusters may in fact have an intermediate age. It is hard to state the statistical significance of this difference given the extremely low numbers and the fact that field AGB stars are distributed all over the galaxy.

#### Appendix D: Surface brightness profiles

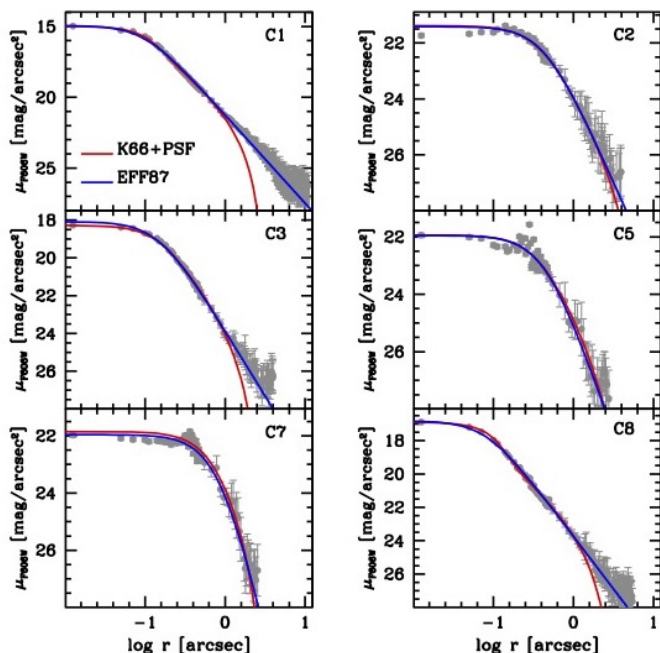


**Fig. D.1.** Surface brightness profiles of the clusters possibly associated with the NGC 5238 tidal tails with over-plotted the best-fit K66 model convolved with a simple model of the HST PSF (red) and EFF87 (blue) models.

The observed SB profile together with the best fit K66 and EFF87 models for the six clusters possibly associated with the tidal tails of NGC 5238 are displayed in Fig. D.1. The adopted EFF87 profiles have the form:

$$\mu(r) = \mu_0 + 1.25\gamma \log\left(1 + \frac{r^2}{\alpha^2}\right) \quad (\text{D.1})$$

where  $\mu_0 \equiv \mu(0)$  (Gatto et al. 2021).

As done in Gatto et al. (2021), the fit of the EFF87 is limited to the SB points out to a limiting radius  $r_f$  that approximately coincide to the last points of the observed profile shown in each panel of Fig. D.1. The structural parameters of the studied clusters, derived from the SB profile fits shown in Fig. D are reported in Table D.1. The half-light radii have been obtained by direct integration of the best-fit profiles.

As a sanity check on the remarkably bright integrated magnitudes of C1, we used APT to measure them also in the SSH LBC images. We obtain  $g = 17.72 \pm 0.06$  and  $r = 17.22 \pm 0.05$ , in the Sloan Digital Sky Survey ABMAG photometric system (Fukugita et al. 1996), calibrated as described in Annibaldi et al. (2020). With the same assumptions on distance and reddening as above, the corresponding absolute magnitudes are  $M_g = -10.42 \pm 0.08$  and  $M_r = -10.90 \pm 0.07$ . The colour  $(g-r)_0 = 0.48 \pm 0.08$  is typical of classical MW GCs (Peacock et al. 2010). Using the transformation

$$V = g - 0.5784(g-r) - 0.0038 \quad (\text{D.2})$$

by Lupton (2005)<sup>12</sup> we obtain  $M_V = -10.7 \pm 0.1$ , compatible with the measure obtained from HST data and, above all, providing a fully independent confirmation of the high luminosity of C1.

This letter is focused on the six clusters that appear to correlate more strictly to the tidal tails of NGC 5238. C4 and C6 were included in our list because they appeared evident in the visual inspection of the galaxy outskirts that lead to the discovery of the new clusters. However, in the present analysis, they play the precious role of a bridge between us and LEGUS since they allowed us to verify that, for these clusters, our newly derived integrated magnitudes are in good agreement with the independent measures by LEGUS (see Sect. 2). In particular, the differences in the integrated magnitudes between our measures and those by LEGUS are  $\Delta F606W = 0.01 \pm 0.10$  and  $\Delta F814W = -0.06 \pm 0.10$  for C4, and  $\Delta F606W = -0.14 \pm 0.09$  and  $\Delta F814W = -0.22 \pm 0.09$  for C6. The fact that our magnitudes are slightly brighter than those by LEGUS is due to the fact that we adopted large apertures, purposely suited to include the contribution by resolved stars, while SExtractor, by definition, should have considered only the unresolved body of the clusters when computing the magnitudes within the LEGUS pipeline. Indeed, the magnitudes we derived from our images with SExtractor more closely match the LEGUS values than those obtained with APT.

Finally, we note that also C6 is quite a bright cluster ( $M_V = -9.55 \pm 0.06$ ), with properties overlapping with those of the faintest NSCs, and it also displays a significant ellipticity,  $\epsilon \simeq 0.25$ , as measured with SExtractor.

<sup>12</sup> <https://www.sdss3.org/dr9/algorithms/sdssUBVRITransform.php#Lupton2005>

**Table D.1.** Structural parameters of the analysed clusters

| SSH<br>id | $r_c^{K66}$<br>arcsec | $R_h^{K66}$<br>arcsec | $C^{K66}$ | $\mu_0^{K66}$<br>mag/arcsec <sup>2</sup> | $\mu_0^{EFF87}$<br>mag/arcsec <sup>2</sup> | $\alpha$<br>arcsec | $\gamma$  | $R_h^{EFF87}$<br>arcsec | $\log L_{F606W}^{EFF87}$<br>$L_\odot$ |
|-----------|-----------------------|-----------------------|-----------|--|--|--------------------|-----------|-------------------------|---------------------------------------|
| C1        | 0.06±0.01             | 0.19±0.03             | 1.70      | 14.97                                    | 14.93±0.12                                 | 0.098±0.005        | 2.50±0.01 | 0.30±0.19               | 6.22±0.07                             |
| C2        | 0.37±0.06             | 0.79±0.12             | 1.35      | 21.37                                    | 21.41±0.06                                 | 0.440±0.024        | 2.59±0.07 | 0.74±0.10               | 4.86±0.07                             |
| C3        | 0.12±0.01             | 0.25±0.02             | 1.35      | 18.28                                    | 18.08±0.08                                 | 0.147±0.006        | 2.76±0.03 | 0.28±0.06               | 5.13±0.05                             |
| C4 (11)   | 0.06±0.01             | 0.17±0.03             | 1.60      | 16.74                                    | 16.45±0.09                                 | 0.077±0.003        | 2.45±0.02 | 0.21±0.06               | 5.45±0.06                             |
| C5        | 0.34±0.08             | 0.60±0.14             | 1.20      | 21.94                                    | 21.95±0.11                                 | 0.440±0.035        | 3.20±0.13 | 0.57±0.14               | 4.34±0.09                             |
| C6 (591)  | 0.06±0.01             | 0.19±0.03             | 1.70      | 15.83                                    | 15.75±0.10                                 | 0.100±0.004        | 3.60±0.01 | 0.25±0.08               | 5.83±0.06                             |
| C7 (617)  | 0.69±0.16             | 0.66±0.15             | 0.70      | 22.03                                    | 21.96±0.06                                 | 0.899±0.065        | 4.94±0.33 | 0.67±0.09               | 4.56±0.08                             |
| C8        | 0.04±0.01             | 0.17±0.04             | 1.90      | 16.89                                    | 16.82±0.15                                 | 0.081±0.005        | 2.53±0.02 | 0.23±0.17               | 5.27±0.08                             |

**Notes.** Numbers in parentheses in the first column are LEGUS id numbers, when available. Central surface brightness values are not corrected for interstellar extinction.  $\log L_{F606W}^{EFF87}$  has been derived by integration to infinity of the best-fit EFF87 model and assuming  $M_{F606W,\odot} = 4.66$  from <https://mips.as.arizona.edu/~cnaw/sun.html>. The K66 parameters have been derived by fitting K66 models convolved with a simple model of the HST PSF to the observed profiles, while EFF87 parameters are derived by fits not taking into account the effect of the PSF on the profile. The uncertainty in  $r_c^{K66}$  has been computed as the range over which the  $\chi^2$  value increases by a factor of 2 with respect to the minimum. C6 is significantly flattened ( $\epsilon \approx 0.25$ , as measured with SExtractor) hence the profile we derived with circular apertures may not be an adequate representation of the real profile.

## Appendix E: Distance and reddening

We derived a new distance estimate for NGC 5238 from the RGB Tip (TRGB) using our ACS photometry. Following exactly the same procedure as Bellazzini & Pascale (2024) we obtain  $F814W_0^{TRGB} = 24.10 \pm 0.01$  and  $(F606W - F814W)_0^{TRGB} = 1.13 \pm 0.06$ . Adopting, from the same authors,  $M_{F814W_0}^{TRGB} = -3.996 \pm 0.045$  for the RGB Tip of the Small Magellanic Cloud that have the same colour, we get  $(m - M)_0 = 28.10 \pm 0.05$ , corresponding to  $D = 4.17 \pm 0.10$  Mpc. At a first glance this is significantly smaller than  $D = 4.51 \pm 0.06$  Mpc by Tully et al. (2009) but, in fact, this is based on a very different calibration and the uncertainty on the calibration is completely neglected, while it is fully taken into account by Bellazzini & Pascale (2024). Moreover, Tully et al. (2009) derive  $F814W_0^{TRGB} = 24.20 \pm 0.02$ , that is hardly compatible with our CMD, even at a first glance. On the other hand, the LEGUS collaboration reports  $D = 4.43 \pm 0.34$  Mpc (Sabbi et al. 2018; Cook et al. 2023), compatible with our measure, within the uncertainties. We do not enter here in the discussion of the merit of the various distance estimates, we simply adopt our own one because is smaller than the others, a conservative choice in the derivation of the absolute integrated magnitude of the clusters in the sense that the values that we obtain are unlikely to be inflated by the adoption of an overly large distance.

The Schlegel et al. (1998) reddening maps show that the foreground extinction is very low and uniform over the field covered by our ACS images and in the extreme outskirts of the galaxy, where the clusters we are interested in are located, there should be no contribution from internal extinction. Consequently we adopt  $E(B - V) = 0.01$ , re-calibrating the mean value from the Schlegel et al. (1998) maps according to Schlafly & Finkbeiner (2011). As a sanity check, these results have been confirmed using the extinction maps by Vergely et al. (2022). We adopt the reddening laws reported in Bellazzini & Pascale (2024).